Journal of Molecular Catalysis A: Chemical 351 (2011) 143–153

Contents lists available at SciVerse ScienceDirect

Journal of Molecular Catalysis A: Chemical

journal homepage: www.elsevier.com/locate/molcata

Tungsten(II)-catalyzed rearrangements of norbornadiene: Effects of alternative complexation stages

Arumugam Jayaraman, Greg M. Berner, Lynn M. Mihichuk, Allan L.L. East*

Department of Chemistry and Biochemistry, University of Regina, Regina, Saskatchewan S4S 0A2, Canada

ARTICLE INFO

Article history:
Received 1 August 2011
Received in revised form
27 September 2011
Accepted 27 September 2011
Available online 5 October 2011

Keywords:
Norbornadiene
DFT
Alkylidene formation
Oxidative coupling
Agostic structures

ABSTRACT

The spontaneous transformation of norbornadiene (nbd, bicyclo[2.2.1]hepta-2,5-diene) to an alkylidene, within a selection of Group 6 organometallic complexes, was studied using density-functional theory computations. This as-yet-unknown mechanism is postulated to be required in the spontaneous ring-opening metathesis polymerization of nbd via Group 6 complexes. In a previous study, an extensive computational search for intermediates and transition states was made for the rearrangement within the originally 7-coordinate $WI_2(CO)_3(\eta^2,\eta^2$-nbd) complex, which we call the Category I searches. In the current study, we perform similar searches but for two other stages of the complex, which we designate Category II and Category III. The Category II searches assume one carbonyl has been dissociated, thus beginning with a 16-electron (16e) complex. The Category III searches assume that the dissociated carbonyl has been replaced by an η^2-nbd, which allows possible coupling of two nbd molecules to form the initial alkylidene needed for polymerization. Category II resulted in activation barriers equally as high as for Category I, if not higher, due to the increased reluctance of the electrophilic metal centre to allow ligands to loosen their metal–ligand bonds for rearrangement. Category III, however, resulted in activation energies half as large as the single-nbd rearrangements of Categories I and II.

1. Introduction

Many Group 6 transition metal complexes are known to be able to catalyze ring-opening metathesis polymerization (ROMP) of norbornadiene (nbd, bicyclo[2.2.1]hepta-2,5-diene) without the requirement of a preformed Schrock type metal alkylidene [1–5]. The accepted ROMP mechanism proceeds via metal-alkylidene and metallacyclobutane intermediates [6]; the perplexing issue is how such an intermediate is first formed *in situ* in these Group 6 cases. In the simpler case of the ROMP of norbornene (nbe, bicyclo[2.2.1]hept-2-ene) utilizing similar catalysts, the activation step is believed [5,7] to be a net 1,2-H-shift along the metal-coordinated C=C double bond to generate an alkylidene, based on experimental evidence [8]. However, nbd offers other possibilities due to its extra degree of unsaturation, and experimental evidence is even less clear-cut [3].

One can envision several possibilities for the coordination in the starting complex that leads directly to the rearrangement to an alkylidene, and in an earlier density-functional-theory (DFT) study we categorized four classes of mechanisms, based on possible initial coordination stages (Fig. 1 below) [9]. That previous study explored Category I mechanisms with the model complex $WI_2(CO)_3(\eta^2,\eta^2$-nbd), and it was concluded that the mechanism is unlikely to be a Category I mechanism, since the computationally predicted overall barrier heights for all path possibilities with this model compound were over 45 kcal mol^{-1} [9].

This current article explores Categories II and III with the same model starting compound and the same level of theory. As we will demonstrate, Category II paths with the dicarbonyl $WI_2(CO)_2(\eta^2,\eta^2$-nbd) have energy barriers at least as high as Category I with the tricarbonyl $WI_2(CO)_3(\eta^2,\eta^2$-nbd), but Category III with $WI_2(CO)_2(\eta^2,\eta^2$-nbd)(η^2-nbd) appears to be able to lower the activation energy in half, to plausible levels. This Category III mechanism involves an oxidative coupling to form a metallacyclopentane, followed by a 1,4-H-shift (between the two α-bonded carbons) across the face of the metal atom. The mechanism was first hypothesized and studied by Handzlik et al. [10,11]; the present study reveals that several minor extra intermediate steps are involved, in which the metallacyclopentane contorts in order to reduce the distance between the α-bonded carbon atoms from 3.3 to 2.6 Å to allow the 1,4-H-shift. The qualitative stages of this mechanism can thus be represented as in Fig. 2.

Herein we will demonstrate that this qualitative mechanism exists for two stereoisomers of our model W complex $WI_2(CO)_2(\eta^2,\eta^2$-nbd)(η^2-nbd), as well as for the Mo complex $MoCl(SnCl_3)(CH_3CN)(CO)(\eta^2,\eta^2$-nbd)($\eta^2$-nbd) studied by Handzlik

* Corresponding author. Tel.: +1 306 585 4003; fax: +1 306 337 2409.
E-mail address: allan.east@uregina.ca (A.L.L. East).

1381-1169/$ – see front matter © 2011 Elsevier B.V. All rights reserved.
doi:10.1016/j.molcata.2011.09.028

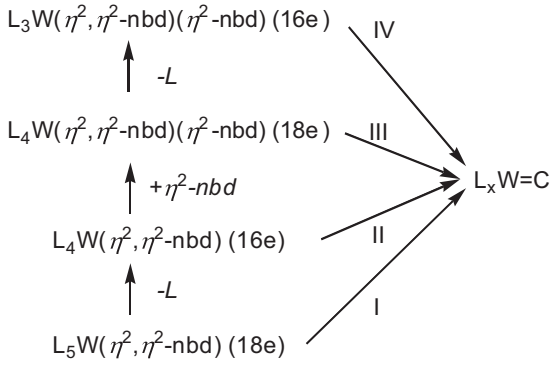

Fig. 1. Four categories (I–IV) for complexation stages during which alkylidene generation might occur. Each category contains several hypothetical mechanisms to be explored; the present work studied Categories II and III.

et al. [11]. We will point out the interesting variations between the paths of the W vs. Mo cases, and suggest that this mechanism be considered a plausible one for *in situ* metal alkylidene formation, worthy of further investigation.

2. Computational details

Calculations were performed with the Gaussian03 (revision C.02 and E.01) and Gaussian 09 (revision B.01) software programs [12]. All energies, including individual-step activation energies E_a and reaction energies ΔE, are reported without zero-point corrections, to be consistent with an earlier study [9]. For the Categories II and III tungsten models $WI_2(CO)_2(\eta^2,\eta^2\text{-nbd})$ and $WI_2(CO)_2(\eta^2,\eta^2\text{-nbd})(\eta^2\text{-nbd})$, the theoretical method used was BP86/RDZP:ITZ2DF:6-31G(d) to be consistent with an earlier study [9]; this method involves the DFT approximation BP86 [13,14], and basis sets RDZP and ITZ2DF for W and I atoms respectively [9], with 6-31G(d) for remaining atoms. For $MoCl(SnCl_3)(CO)(NCMe)(\eta^2,\eta^2\text{-nbd})(\eta^2\text{-nbd})$, the method used was B3LYP/LANL2DZ, to be consistent with an earlier study [11]; the DFT approximation here is B3LYP [15,16]. The STO-3G minimal basis set was used for the C and H atoms of dppm (bis(diphenylphosphino)methane) when this ligand was used.

Transition-state calculations used the algorithm opt = (ts, noeigentest, calcfc) [17,18]. Each optimized transition state was tested in our usual way, verified with vibrational frequency calculations, and connected to other reaction steps via plus/minus-displacement energy-minimization runs [9]. Cartesian coordinates for all transition states appear in Appendix A.

Effects of solvation in toluene were estimated by computing Gaussian09 single-point energies of the molecules surrounded by a continuum dielectric (SCRF = IEFPCM, solvent = toluene) [19]. Only the default electrostatic effect is included.

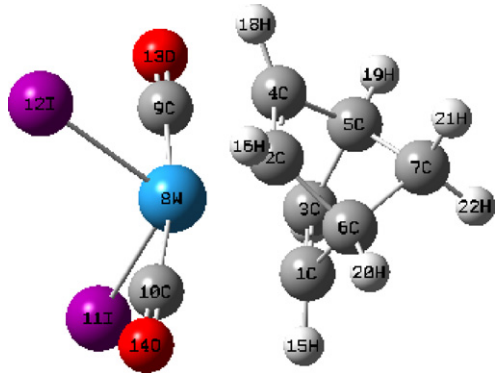

Fig. 3. Atom numbering of Baker's stereoisomer of $WI_2(CO)_2(\eta^2,\eta^2\text{-nbd})$ for Table 1.

Table 1
Internal coordinates of Baker's stereoisomer of $WI_2(CO)_2(\eta^2,\eta^2\text{-nbd})$ (Å,°).

Coordinate[a]	Us (DFT)	Baker (expt)[b]	Error
C1–W–C4	74.1	73.4 (73.1,73.7)	0.7
C1–W–C2	62.3	61.9 (61.3,62.4)	0.5
C1–W–C3	36.0	35.5 (34.8,36.2)	0.5
C1–W–I12	152.0	153.7 (152.2,153.6,154.1,154.7)	−1.6
C1–W–I11	92.2	94.6 (94.2,94.6,94.7,95.0)	−2.4
C10–W–I11	87.1	87.1 (86.5,86.7,86.8,88.5)	0.0
C10–W–C3	112.2	111.7 (111.2,111.3,112.2,112.2)	0.5
C10–W–C1	76.2	76.2 (75.1,76.0,76.4,77.4)	0.0
C10–W–C9	170.0	170.5	−0.5
I11–W–I12	109.6	104.9	4.7
rms error			***1.8***
W–C1	2.307	2.291 (2.270,2.285,2.292,2.318)	0.016
W–C10	2.031	2.068 (2.067,2.068)	−0.036
W–I11	2.711	2.704 (2.703,2.704)	0.007
rms error			***0.023***

[a] For atom numbering see Fig. 3.
[b] Ref. [4].

3. Results for Category II: $WI_2(CO)_2(\eta^2,\eta^2\text{-nbd})$

3.1. Reproduction of Baker's stereoisomer

Our level of approximation reproduces well the X-ray crystal structure of $WI_2(CO)_2(\eta^2,\eta^2\text{-nbd})$ of Baker et al. [4], as shown in Fig. 3 and Table 1, with rms errors of 0.023 Å for bond lengths to W and 1.9° for bond angles involving W. This level of accuracy was expected, based on our earlier tests of this level of theory [9]. Note that the crystal deformations cause deviations from C_{2v} symmetry that span ranges of up to 2°. Our unscaled CO-stretch vibrational frequencies (cm^{-1}) of 1985 and 2042 match well the measured values of 1982 and 2058 [4].

This lowest-energy stereoisomer of $WI_2(CO)_2(\eta^2,\eta^2\text{-nbd})$ was not used in the mechanism study because it is a "cis,cis,trans" stereoisomer (for the C=C, I, "other" attachments). The relevant

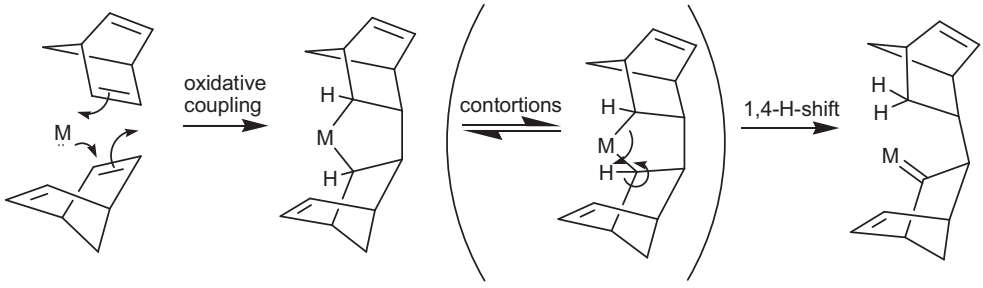

Fig. 2. The lowest-energy mechanism for metal alkylidene formation calculated to date, as determined in this work.

Table 2
Computed relative energies (kcal mol^{-1}) for Category II intermediates.

Structure	*E*	Structure	*E*	Structure	*E*
1a	0.0	**8d**	21.8	**16b**	29.6
1b	1.9	**9a**	12.8	**16c**	13.2
1c	1.9	**9b**	22.3	**20a**	19.7
2a	17.4	**9c**	19.6	**20b**	11.9
6a	6.9	**10a**	17.0	**20c**	13.9
6b	6.6	**10b**	17.7	**20d**	14.5
6c	8.3	**14a**	29.2	**24**	42.8
8a	10.7	**14b**	32.5	**26a**	36.3
8b	20.7	**14c**	44.7	**26b**	40.9
8c	21.5	**16a**	17.5		

experiments with the dppm ligand produced the isolable intermediate $WI_2(CO)(dppm\text{-}\kappa^2P)(\eta^2,\eta^2\text{-nbd})$ in a "cis,cis,cis" arrangement [20]. Hence, for the Category II study, we began with an alternate stereoisomer in which the two CO ligands are cis to each other.

3.2. Summary of intermediates found

See Fig. 4 and Table 2. We have some new structures not seen in Category I studies [9]; **24** features the hydrocarbon in a tridentate form, **25** is a curious "shelf state" (almost but not quite a PES minimum) at our level of approximation, and **26** is an agostic form. These three forms are undoubtedly due to the more electrophilic W due to loss of a ligand from $WI_2(CO)_3(\eta^2,\eta^2\text{-nbd})$ in the Category I studies. This loss of a ligand also results in many agostic interactions, with 3-centre-2-electron W–C–H regions, which were not evident in Category I intermediates. Further proof of the increased electrophilicity of W in Category II comes from the computed dissociation energies for $WI_2(CO)_n(\eta^2,\eta^2\text{-nbd}) \rightarrow WI_2(CO)_n + nbd$ at our level of theory: 24 kcal mol^{-1} for $n=3$ but 45 kcal mol^{-1} for $n=2$. Relative energies of these Category II intermediates are generally slightly higher than those of Category I, indicating greater relative stability of 16e vs. 14e complexes than 18e vs. 16e complexes; one exception is a backbiting version of **8** (**8a**) which is particularly stable in Category II.

3.3. Rearrangements via C–H insertion

See Fig. 5. The most important observation is that the barriers for rearrangement to metal carbene have not changed from those of Category I. The lowest-energy path, via η^2-nbd and agostic-W–C–H intermediates, has an overall barrier of 49 kcal mol^{-1}, higher than the one-step 45.6 kcal mol^{-1} barrier of Category I computations. Hence, loss of a ligand does not qualitatively change the energy barrier to these rearrangements.

3.4. Rearrangements via C–C insertion

See Fig. 6. Again, as in Category I, the C–C insertion paths did not result in any significant changes to overall barrier heights. The lowest-energy path here, via π-allyl structure **20d** to carbene **9b**, produced an overall E_a of 53.7 kcal mol^{-1}, slightly larger than the lowest-energy Category I path at 51.0 kcal mol^{-1} (which went via π-allyl structures as well). There were some qualitative differences of note: in the Category I C–C insertion paths, the barrier to quadricyclane-inserted complex **16** was low and the barrier to π-allyl complex **20** was high (respectively 14 and 55 kcal mol^{-1}), but in Category II these intermediates could be achieved via similar barriers (30 and 35 kcal mol^{-1}, respectively).

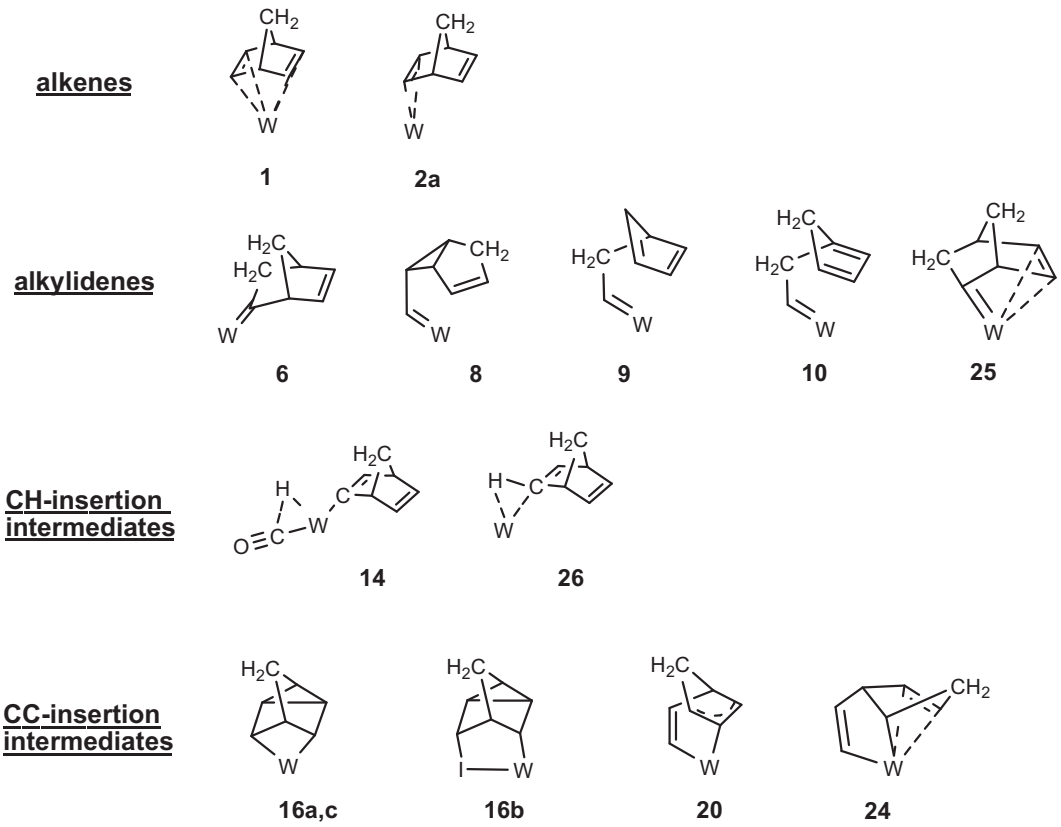

Fig. 4. Structures found as intermediates (local minima) for Category II in this work. Numbering is kept consistent with Ref. [9]. Note that **25** is not a local minimum (but a "shelf state") at our level of theory.

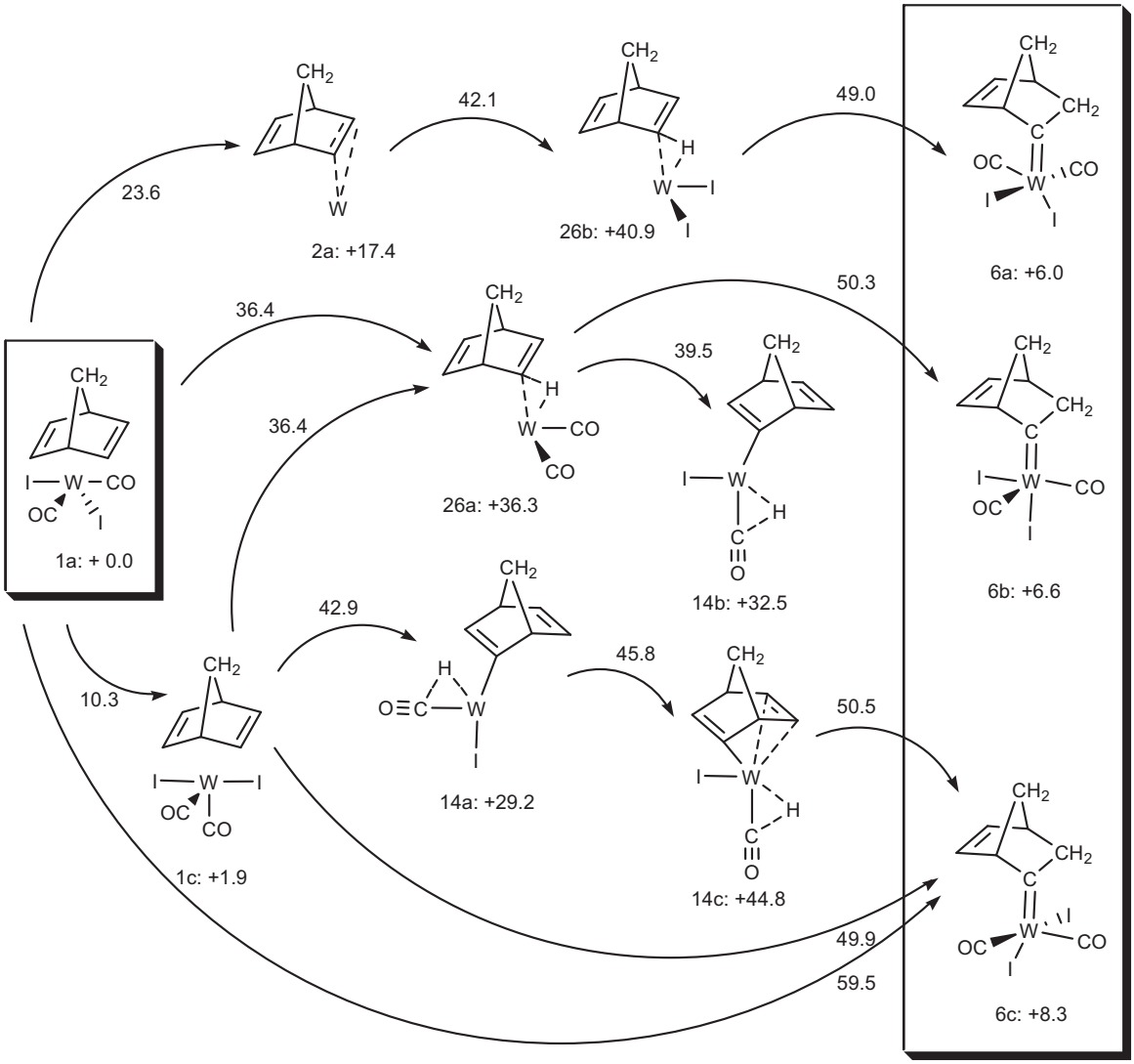

Fig. 5. Reaction pathways via C–H insertion as found computationally. CO and I ligands are generally omitted from sketches for clarity. Alkylidene structures are in the boxed area on the right. All energies are in kcal mol^{-1}; the ones alongside reaction arrows represent transition-state energies relative to **1a** (i.e., not individual-step barrier heights).

4. Results for Category III: $WI_2(CO)_2(\eta2,\eta2\text{-nbd})(\eta2\text{-nbd})$

4.1. Initial stereoisomer search

Four cis–cis–cis stereoisomers of $WI_2(CO)_2(\eta^2,\eta^2\text{-nbd})(\eta^2\text{-nbd})$ (**27**) were initially optimized (**27a–d**, Fig. 7). All four structures adopt a slightly distorted pentagonal–bipyramidal spatial arrangement about the W atom. The BP86 relative energies of the 4 stereoisomers are 0.0, 2.3, 12.6, and 21.7 kcal mol^{-1}, respectively. The two lowest-energy stereoisomers **27a** and **27b** are the ones with a carbonyl in an axial position. The trans effect of the axial carbonyl results in very weak η^2 interaction between the axial η^2-nbd unit and W atom (averaged W–C9 and W–C10 distances for **27a** and **27b** are >2.8 Å, while for **27c** and **27d** they are <2.6 Å), which reduces steric crowding. They also have more attractive eq–eq interactions between iodine I17 and the carbonyl carbon C19 than the higher-energy stereoisomers do; the bond angles I17–W1–C19 for **27a–d** are 62°, 63°, 73° and 67°, respectively, the angles W1–C19–O21 are 166°, 167°, 171° and 171°, respectively, and the interatomic distances C19–I17 are 2.69, 2.68, 2.99 and 2.82 Å, respectively.

We used the lowest energy isomer **27a** for study of the mechanistic pathway for metal alkylidene generation. The lowest-energy mechanism found, a 1,4-H-shift pathway, was then also explored for the alternative **27b** stereoisomer, but this did not lead to a reduction in overall activation energy (see Appendix A).

4.2. C–C-rearrangement pathways

We pursued two qualitatively different types of paths: one using 6e rearrangements, and the other using primarily 4e rearrangements. Fig. 8 presents the lowest-energy path of each style. Both presented paths start with the low-barrier oxidative coupling of the two nbd units to form the 5-membered metallacycle **28**, an endothermic step with an energy difference of ΔE = 7.6 kcal mol^{-1}, and E_a = 15.8 kcal mol^{-1} [**TS**(**27a** → **28**)] as an activation energy barrier. Oxidative coupling of alkene ligands and the formation of metallacyclopentane is experimentally known [21,22] and has been analyzed theoretically [23,24]. Structure **28** has a very weak η^2 interaction between the metal and the olefinic carbons C7=C8; the distances between W1–C8 and W1–C7 are 2.5 Å and 2.8 Å, respectively. The second step to **29** is a minor adjustment to add the metal–π interaction to the C7=C8 double bond.

From **29**, Path A involves two more 6-electron rearrangements steps. The step **29** → **30** moves three pairs of electrons from W–C3,

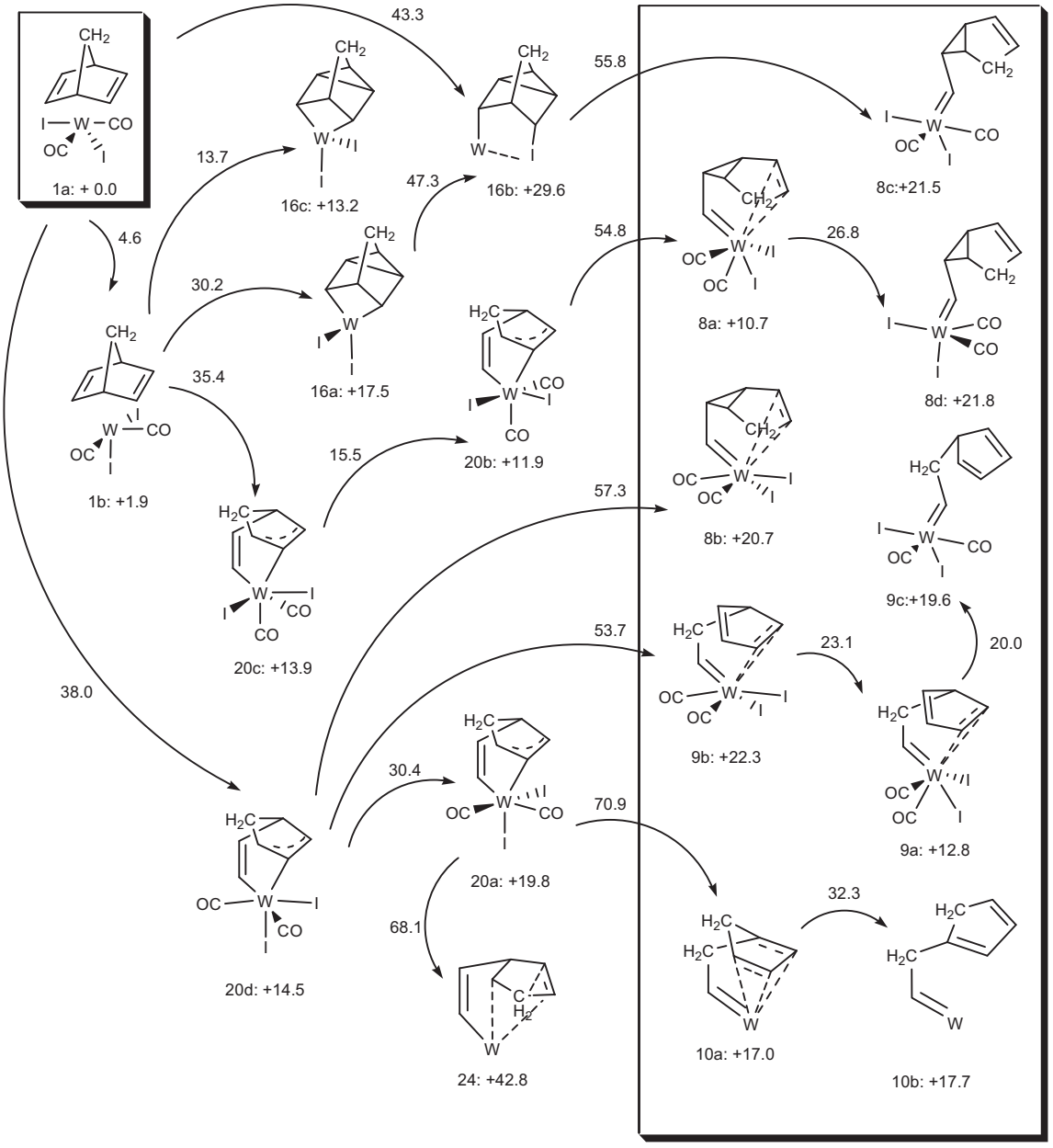

Fig. 6. Reaction pathways via C–C insertion as found computationally. CO and I ligands are generally omitted from sketches for clarity. Alkylidene structures are in the boxed area on the right. All energies are in kcal mol^{-1}; the ones alongside reaction arrows represent transition-state energies relative to **1a** (i.e., not individual-step barrier heights).

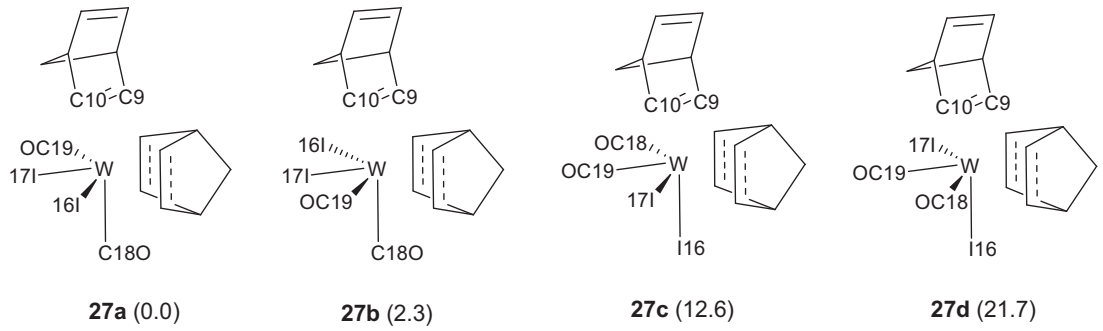

Fig. 7. Four different stereoisomers of $WI_2(CO)_2(\eta^2,\eta^2\text{-nbd})(\eta^2\text{-nbd})$, with relative BP86 energies (kcal mol^{-1}) in parentheses. Lower energies are observed when η^2-nbd is trans to a CO in axial positions.

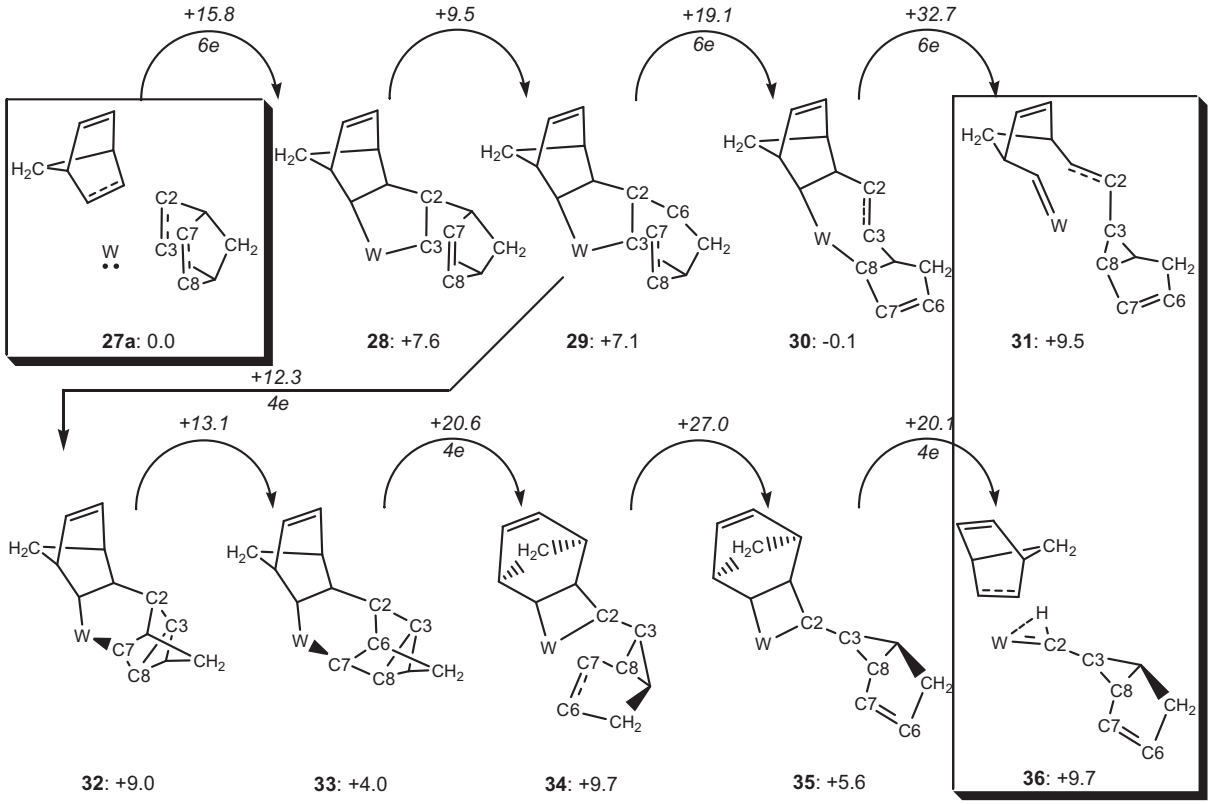

Fig. 8. Category III C–C-rearrangement pathways: Path A (top row) involves 6e rearrangements. Path B starts with the same 6e oxidative coupling rearrangement **27a** → **28** and adjustment to **29**, and then involves 4e rearrangements (bottom row). Dashed bonds indicate metal–π interaction. Numbers indicate BP86 energies (kcal mol^{-1}) relative to **27a**. Two CO and two I ligands not shown, for clarity.

C2–C6, and C7–C8 to W–C8, C6–C7, and C2–C3, which creates a 7-membered metallacycle with a metal–π interaction to the C2=C3 double bond. From structure **30** we found two ways to form a metal carbene, by breaking a C–C bond on either (a) the non-rearranged nbd moiety or (b) the C4–C8 bond on the 5-membered ring. The step presented in Fig. 8 is option (a), which had a 5.7 kcal mol^{-1} lower activation energy than (b). The overall barrier height for this 4-step pathway is 32.7 kcal mol^{-1}.

Path B involves 5 more steps from **29**: three 4e rearrangements, separated by additional minor geometrical adjustment steps. The 4e rearrangement from **29** to **32** involves W1, C3, C7, and C8, creating a metal-inserted quadricyclane moiety and a 6-membered metallacycle. Structure **32** has a tight W1–C7–C8 angle of 81°, indicating some residual metal–π character. The adjustment from **32** to **33** releases this residual metal–π character, as the W1–C7–C8 angle expands from 81° to 124°, and the bonds in the 3-membered ring tighten. The ensuing 4e rearrangement **33** → **34** involves W1, C2, C6, and C7, generating a C6=C7 double bond with metal–π interaction, and a 4-membered metallacycle. After an adjustment to break the η^2 metal–π interaction in **34**, the pathway completes with **35** → **36**, a Chauvin 4e rearrangement to metal carbene **36**. This 4e step is endothermic with activation energy of 14.5 kcal mol^{-1}, and hence similar to the BP86-computed results for a ruthenocyclobutane case by Rowley et al. (E_a values of 5.0 and 16.2 kcal mol^{-1}) [25]. The overall barrier height for this 7-step pathway is 27.0 kcal mol^{-1}.

Note that in Path B the additional η^2-nbd would appear to behave as a co-catalyst, unlike in Path A. In fact, if Path B were to occur, it might instead travel only to the metallacyclobutane **34** and then proceed immediately with ROMP, which first takes **34** to alkylidene **31** instead of alkylidene **36**.

4.3. 1,4-H-shift pathway

This pathway, first explored by Handzlik et al. for a Mo complex [11], generated the lowest overall activation energy we have yet found for the nbd → alkylidene rearrangement: +15.8 kcal mol^{-1}. This is substantially lower than the C–C rearrangement pathways found above, and one-third of the activation energies arising from Categories I and II rearrangements. For the transformation of metal alkene **27a** to the corresponding metal alkylidene **45** via 1,4-H-shift, we found 10 different intermediates (local minima **28**, **29**, **37**–**44**) connected by 14 transition states along several paths. The resulting pathways are shown in Fig. 9, where we have grouped the intermediates into classes for ease of discussion. The computed potential energy profiles are shown in Fig. 10 and internal coordinate values are listed in Table 3.

All the located 1,4-H-shift pathways start with the same oxidative coupling step **27a** → **28** of the C–C rearrangement pathways. The difference here vs. Fig. 8 is that **TS**(**27a** → **28**) is the *highest-energy point* in the potential energy profile of the best 1,4-H-shift pathway.

The second stage of the pathways here is a set of contortions that reduce the distance between C3 and C10 from 3.3 to 2.6 Å (**28** → **41**), to allow the third stage of reaction, the 1,4-H-shift from C3 to C10. This second stage from **28** to **41** can be achieved by three different pathways (Fig. 9). Pathway (i) involves the conversion through a higher-energy intermediate, **37**, where the weak η^2 interaction between W and the olefinic bond C7=C8 is broken first, and the strong α-agostic bonds W1–H31–C10 and W1–H23–C3 are formed in ensuing steps. Pathway (ii) is a three-step contortion path as well, but through a lower-energy intermediate, **39**, where the α-agostic W1–H31–C10 bond formation is now

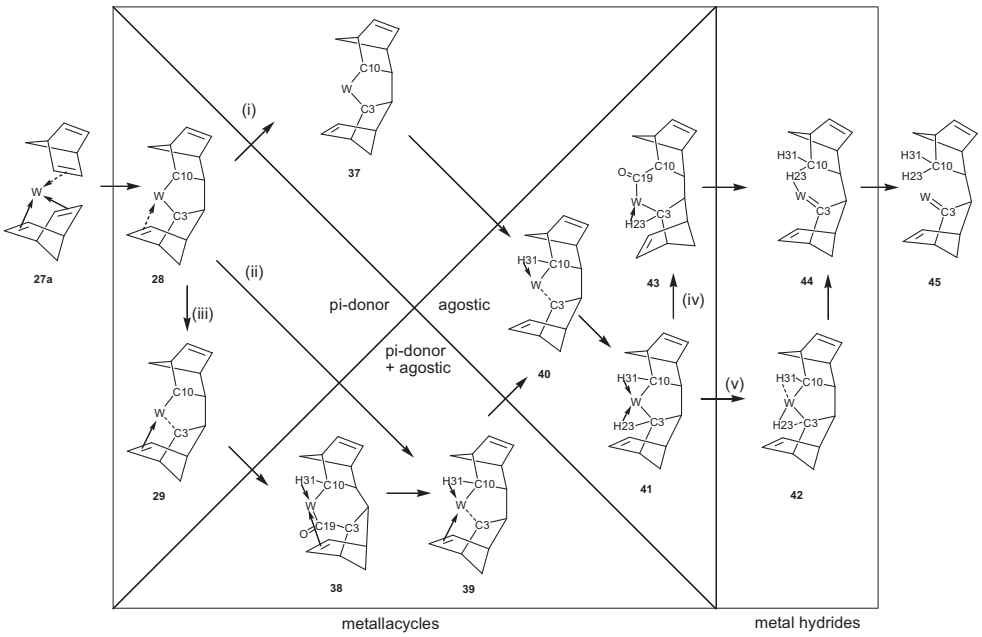

Fig. 9. Various pathways found for the transformation of complex **27a**–**45**. Lowest energy pathway is the bottom most one.

Table 3
Selected computed bond lengths (Å) and bond angles (°) along the lowest-energy path for the Category III rearrangement **27a** → **45**.

Complex	R(W1–C3)	R(W1–C10)	R(W1–C7)	R(W1–C8)	R(C3–C10)	R(W1–H23)	θ(W1–C3–H23)	R(W1–H31)	θ(W1–C10–H31)
27a	2.351	2.878	2.368	2.410	4.765	3.002	116.5	3.016	86.6
TS(**27a**–**28**)	2.199	2.242	2.625	2.490	3.764	2.940	122.9	2.740	105.1
28	2.160	2.144	2.816	2.516	3.312	2.938	125.7	2.720	109.8
TS(**28**–**29**)	2.242	2.160	2.608	2.544	3.215	2.978	122.6	2.699	107.4
29	2.340	2.167	2.254	2.380	3.034	3.052	121.1	2.615	101.3
TS(**29**–**38**)	2.420	2.146	2.204	2.283	2.895	3.144	122.3	2.483	94.1
38	3.126	2.149	2.349	2.339	3.018	4.119	149.9	2.198	77.1
TS(**38**–**39**)	2.584	2.191	2.270	2.240	2.870	3.455	135.5	2.148	72.7
39	2.370	2.204	2.384	2.335	2.779	3.055	118.7	2.217	75.8
TS(**39**–**40**)	2.354	2.151	3.404	2.911	2.752	2.978	114.1	2.239	79.4
40	2.378	2.132	4.271	3.690	2.792	2.914	108.0	2.207	78.5
TS(**40**–**41**)	2.114	2.143	4.439	3.859	2.576	2.176	77.1	2.073	77.5
41	2.114	2.170	4.578	3.994	2.610	1.880	61.9	2.110	71.6
TS(**41**–**42**)	2.095	2.187	4.629	4.029	2.613	1.737	53.3	2.191	75.1
42	2.089	2.211	4.670	4.079	2.636	1.714	47.7	2.316	80.7
TS(**42**–**44**)	2.033	2.372	4.667	4.047	2.640	1.711	47.3	2.656	92.2
44	1.960	2.595	4.534	3.846	2.677	1.713	46.9	2.929	96.5
TS(**44**–**45**)	1.958	2.647	4.531	3.839	2.688	1.728	48.5	2.891	91.4
45	1.961	3.862	4.551	3.812	3.348	3.496	82.6	3.728	74.8

first, and cleavage of the η^2 interaction between W1 and C7=C8 is now the second step. Both these paths require more energy than is required to do the initial oxidative coupling stage alone.

Pathway (iii), the lowest-energy of the three pathways in stage two, is a 5-step contortion which keeps activation energies low by incorporating carbonyl insertion and carbonyl de-insertion steps. The minor first step (**28** and **29**) strengthens the η^2 interaction

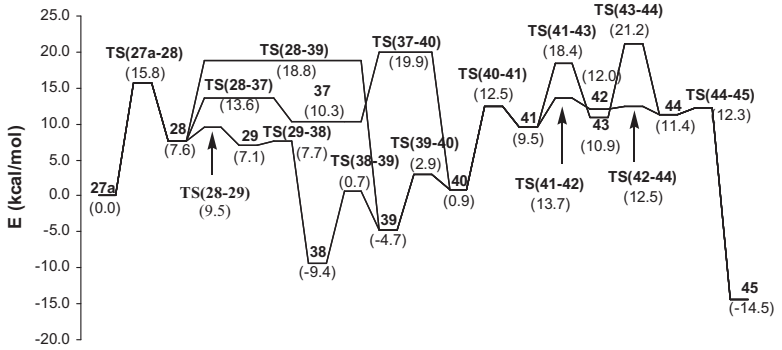

Fig. 10. Potential energy profile for the **27a** → **45** pathways in Fig. 9. The energy values (kcal mol^{-1}) relative to reactant (**27a**) are given in parentheses.

Table 4
Relative energies (kcal mol^{-1}) for Category III path, in vacuum vs. in toluene.

Complex	E_{rel}^{gas}	E_{rel}^{solv}
27a	0.0	0.0
TS(27a–28)	15.8	15.1
28	7.6	6.8
TS(28–29)	9.5	8.9
29	7.1	7.1
42	12.0	12.5
TS(42–44)	12.5	12.9
44	11.4	12.0
TS(44–45)	12.3	12.7
45	−14.5	−13.6

while weakening the W1–C3 bond in the metallacyclopentane. From **29**, the first of the strong α-agostic interactions is created (W1–H31–C10) but in tandem with a strain-relieving migratory-insertion process, forming the complex **38**. The E_a for this step is small (0.6 kcal mol^{-1}) and ΔE is exothermic (−16.5 kcal mol^{-1}). The third step, **38** → **39**, involves the de-insertion of the carbonyl, resulting in a metallacyclopentane intermediate with strong α-agostic and strong η^2 interactions. The fourth and fifth steps are common to pathway (ii): breaking the η^2 interaction, and adding the second α-agostic one.

The third and final stage of the reaction, **41** → **45**, involves the 1,4-H-transfer of newly agostic H_{23} in **41** from C3 to C10. This can be achieved by two different paths (Fig. 9). The higher-barrier path (iv) begins with cleavage of the W1–C10 bond and the associated α-agostic W1–H31–C10 interaction, **41** → **43**, employing a carbonyl migratory insertion to do it, and is followed by α-hydride elimination to form the unstable metal hydride **44**, and an exothermic reductive elimination to form the metal alkylidene **45**. However, the carbonyl migratory insertion is not needed in the lower-energy path (v), **41** → **42** → **44** → **45**. Along this path, α-hydride elimination occurs first (**41** → **42**), with cleavage of the W1–C10 bond and the associated α-agostic W1–H31–C10 interaction in the second step (**42** → **44**), and, like path (iv), it finishes with the same reductive elimination step (**44** → **45**).

Thus, the Category III lowest-energy path for **27a** → **45** on the BP86 potential energy surface has a calculated ΔE = −14.5 kcal mol^{-1}, and the highest-barrier step is the formation of the initial metallacyclopentane (**27a**–**28**) by oxidative coupling, which takes place with a barrier of 15.8 kcal mol^{-1}. Solvent-effect calculations were performed for several steps along this path, and the effects are rather small (Table 4).

5. Results for MoCl(SnCl$_3$)(CO)(NCMe)(η^2,η^2-nbd)(η^2-nbd)

Handzlik et al. had investigated the transformation of nbd within 7-coordinate Mo-containing complexes MoCl(SnCl$_3$)(CO)X$_2$(η^2,η^2-nbd), X = {CO, NCMe, η^2-nbd}, with the B3LYP/LANL2DZ level of theory [11]. These Mo complexes are similar to our W complexes in that the metal is Group 6 and, it could be argued, in a +2 oxidation state (herewith 2 anionic ligands Cl$^-$ and SnCl$_3^-$). Their Category I rearrangements are qualitatively similar to ones we observed with WI$_2$(CO)$_3$(η^2,η^2-nbd) [9]. They also investigated a Category III 1,4-H-shift pathway with MoCl(SnCl$_3$)(CO)(NCMe)(η^2,η^2-nbd)(η^2-nbd) (**46**, Fig. 11), which motivated us to explore the same idea for **27a**, but they presented the mechanism as having only two steps. Since our pathways for **27a** → **45** formally involve 7–9 elementary steps, we were curious why theirs was only 2-step, and we reinvestigated their system at their level of theory.

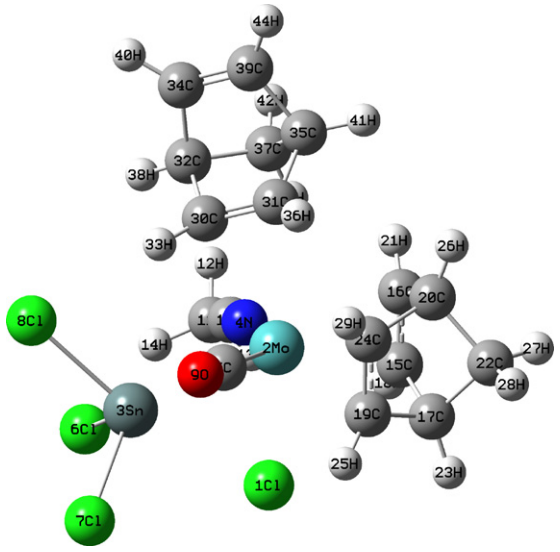

Fig. 11. The B3LYP/LANL2DZ optimized structure of molybdenum(II) complex **46**.

Our results show that they indeed had presented the two important steps in the pathway, and only omitted presenting the connecting contortion steps, which for this case are nearly barrierless. The pathway at their level of theory formally involves 7 steps (here **46** → **53**), similar to the tungsten case **27a** → **45**. Fig. 12 shows a schematic representation of the structures along the pathway, Fig. 13 is the potential energy profile for this transformation, and Table 5 lists the important internal coordinate values.

The opening step of oxidative coupling, **46** → **47**, is very similar to **27a** → **28** as far as the hydrocarbon is concerned, since the 1,4-C15–C30 distance is initially created at 3.4 Å in **47** (3.3 Å in **28**) and there is still a metal–π interaction with the equatorial nbd, with Mo–C19 and Mo–C24 distances of 2.6 and 2.8 Å (2.5 and 2.8 Å in **28**). In the second stage, steps **47** → **48** → **49** → **50** → **51** → **52** are contortions referred to in parentheses in Fig. 2; they involve small geometrical rearrangements which reduce the 1,4-C15–C30 distance from 3.4 to 2.7 Å (3.3–2.6 Å in **28** → **41**). The whole pathway from **47** → **52** involves no strong agostic interactions, but two weak ones (Mo–H18–C15 and Mo–H33–C30) which we might tentatively call "α-anagostic" interactions [26]. The η^2 interaction with the originally equatorial nbd is broken only very late, in the step **51** → **52**. The final stage is a single-step 1,4-H-atom transfer, **52** → **53**, which does not involve metal-hydride intermediates as in **41** → **45**. Simple steric crowding around Mo is likely responsible for this qualitative difference. Overall, the largest-barrier step for the whole path is the 1,4-H-transfer step (**52** → **53**) with E_a = 20.3 kcal mol^{-1}.

Despite the similarities between the pathways for the 1,4-H-shifts of **27a** and **46**, there are some dissimilarities: (i) the W-complex pathways involve 3-centre-2-electron-bonded agostic interaction but the Mo-complex pathway does not, (ii) the 1,4-H-shift step is a single step for **46**, but for complex **27a** it involves shallow-well metal-hydride intermediates and ensuing reductive elimination, (iii) the highest-barrier step in the mechanism is the initial formation of metallacyclopentane for the W-complex, but the direct 1,4-H-shift for the Mo-complex. The origins of these dissimilarities were probed with some exploratory B3LYP/LANL2DZ optimizations of **40** and **52**, but where the W and Mo atoms were interchanged. The resulting structures showed almost *no dependence* on the metal atom identity, and hence the dissimilarities must be due to the ligand sets.

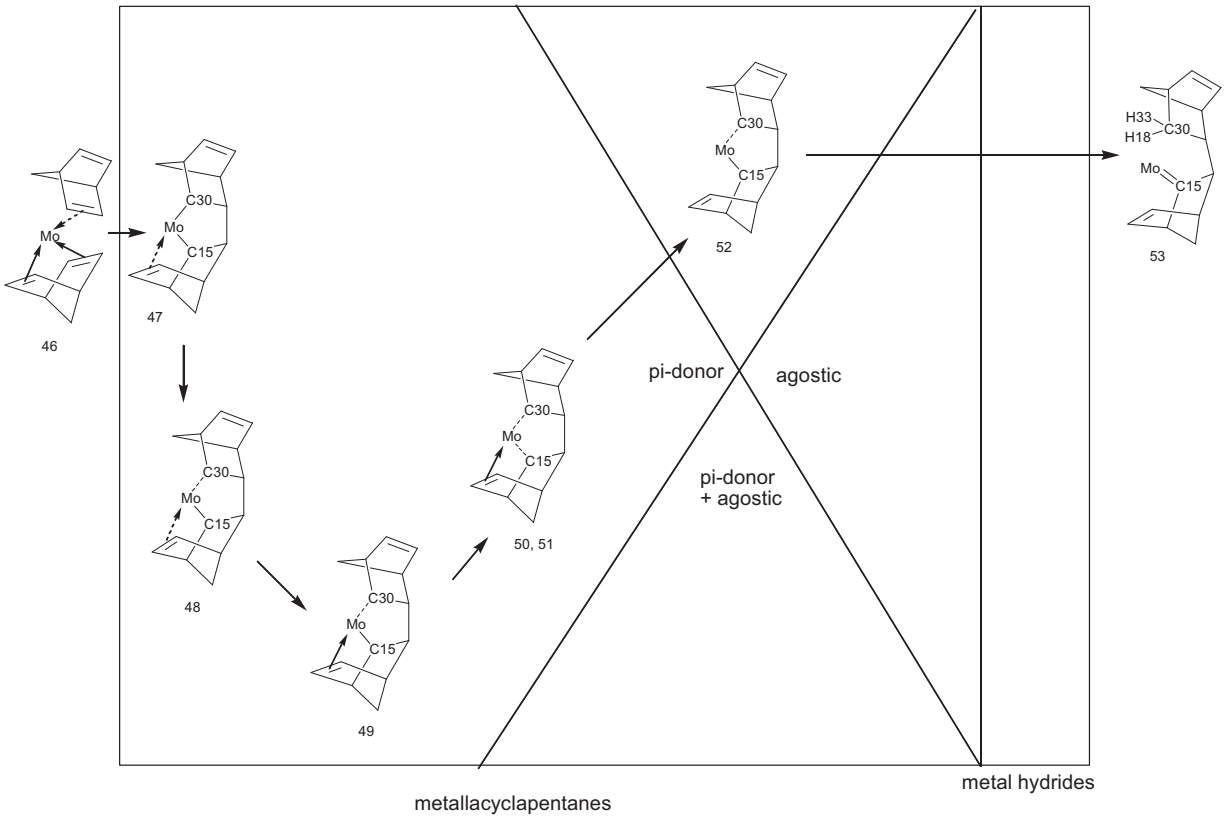

Fig. 12. Schematic representation of the molecular structures found for the transformation of metal alkene **46** to corresponding metal alkylidene **53**.

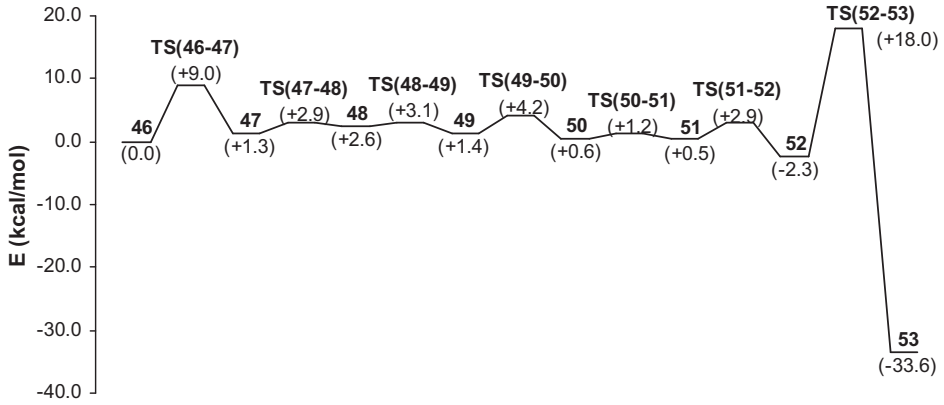

Fig. 13. Potential energy profile for the gas-phase formation **46** → **53**. The energy values (kcal mol^{-1}) relative to reactant (**46**) are given in parentheses.

Table 5
Selected computed bond lengths (Å) and bond angles (°) for the **46** → **53** transformation.

Complex	R(Mo2–C15)	R(Mo2–C30)	R(Mo2–C24)	R(Mo2–C19)	R(C15–C30)	R(Mo2–H18)	θ(Mo2–C15–H18)	R(Mo2–H33)	θ(Mo2–C30–H33)
46	2.424	2.675	2.358	2.319	4.569	2.893	104.6	2.955	94.0
TS(**46**–**47**)	2.186	2.242	2.634	2.532	3.776	2.811	114.3	2.816	110.7
47	2.122	2.146	2.809	2.590	3.367	2.818	119.2	2.788	115.1
TS(**47**–**48**)	2.142	2.210	2.830	2.431	3.050	2.833	118.8	2.795	111.1
48	2.148	2.257	2.777	2.346	2.880	2.793	115.3	2.795	108.0
TS(**48**–**49**)	2.128	2.274	2.591	2.230	2.819	2.774	115.3	2.832	109.4
49	2.133	2.384	2.472	2.163	2.775	2.798	116.8	2.976	112.5
TS(**49**–**50**)	2.201	2.299	2.460	2.229	2.754	2.854	116.2	2.898	112.6
50	2.253	2.260	2.498	2.323	2.716	2.800	108.7	2.866	112.9
TS(**50**–**51**)	2.250	2.255	2.504	2.334	2.689	2.784	107.8	2.848	112.0
51	2.243	2.260	2.509	2.336	2.691	2.777	107.8	2.852	112.0
TS(**51**–**52**)	2.202	2.291	3.151	2.672	2.672	2.702	105.0	2.889	112.6
52	2.135	2.283	3.974	3.278	2.660	2.632	104.2	2.880	112.3
TS(**52**–**53**)	1.963	2.647	4.295	3.583	2.714	1.766	58.8	3.035	100.2
53	1.912	3.707	4.611	3.901	3.236	3.128	76.1	3.716	82.1

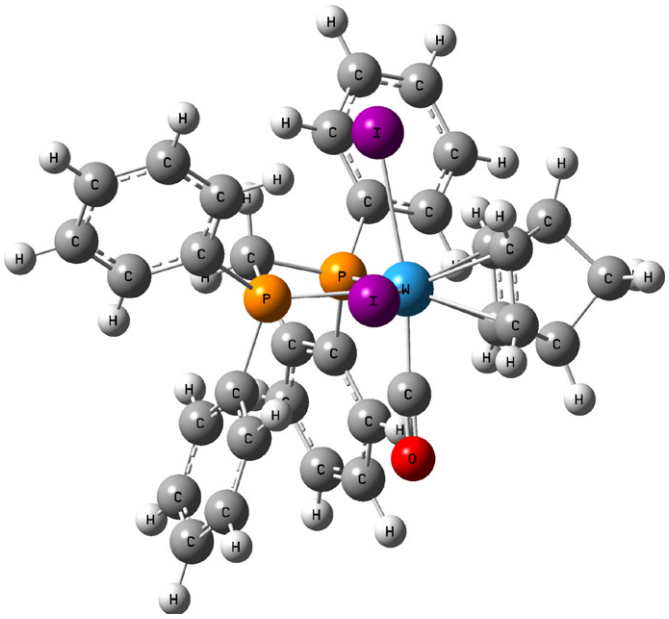

Fig. 14. The BP86 optimized structure of $WI_2(CO)(dppm\text{-}\kappa^2P)(\eta^2,\eta^2\text{-nbd})$.

Table 6
BP86 energies (kcal mol^{-1}) of intermediates of three tungsten(II) systems, relative to the energy of separated reactants.

Reaction	TS	28	39	42	45
$WI_2(CO)_2(\eta^2,\eta^2\text{-nbd})$ + nbd	15.1	6.0	−6.3	10.4	−16.0
$WI_2(dppm\text{-}\kappa^2P)(\eta^2,\eta^2\text{-nbd})$ + nbd	20.7	−2.5	−4.1	7.9	−17.4
$WI_2(CO)(dppm\text{-}\kappa^1P)(\eta^2,\eta^2\text{-nbd})$ + nbd	13.9	1.4	−10.6	−0.6	−22.9

6. Relevance to known W(II) systems

Complex **27a** is a model system. The system used in experiments here in Regina arose from adding nbd to a solution of $WI_2(CO)_3(dppm)$, from which crystals of $WI_2(CO)(dppm\text{-}\kappa^2P)(\eta^2,\eta^2\text{-nbd})$ (shown in Fig. 14) were obtained [20]. We performed some calculations with the dppm-containing complex to prove that the intermediates found here for the model system are valid for the known system.

To make room for an incoming η^2-nbd, an existing W–L connection must be broken from the assumed starting complex. One idea is to remove carbonyl, leading to $WI_2(dppm\text{-}\kappa^2P)(\eta^2,\eta^2\text{-nbd})(\eta^2\text{-nbd})$, while a second idea is the reduction of denticity of dppm, leading to $WI_2(CO)(dppm\text{-}\kappa^1P)(\eta^2,\eta^2\text{-nbd})(\eta^2\text{-nbd})$. Both ideas were examined for structures **27a**, **28**, **39**, **42**, **45**, and the transition state for the early oxidative coupling step. There were minor qualitative differences regarding this oxidative coupling step: in the model it connected **27a** → **28**, but in idea 2 it connected dissociated reactants (6-coordinate complex plus nbd) to **28**, and in idea 1 it connected dissociated reactants to **39**. Gratifyingly, both the existence and the relative energies of this TS and the other intermediates are all in general accord. Table 6 compares their relative energies, when rezeroed to the energy of dissociated reactants.

7. Conclusions

Alternative mechanisms for the spontaneous transformation of norbornadiene (nbd) to an alkylidene have been studied with BP86 DFT calculations for a selection of Group 6 organometallic complexes, since Category I transformations had high (>40 kcal mol^{-1}) activation energies. The Category II searches, which assume one carbonyl has been dissociated, resulted in activation barriers equally as high as for Category I, if not higher, due to the increased reluctance of the electrophilic metal centre to allow ligands to loosen their metal–ligand bonds for rearrangement. The Category III searches, which assume that a dissociated ligand has been replaced with an η^2-nbd, resulted in activation energies half as large as the single-nbd rearrangements of Categories I and II.

The Category III mechanism of oxidative coupling followed by a 1,4-H shift, first hypothesized by Handzlik et al. [10,11], is now the lowest-barrier mechanism we have found to date for the spontaneous formation of alkylidene. We now intend to conduct new benzaldehyde carbene-trapping experiments with our W(II) system, as we have done before with other catalysts [5], to test this new hypothesis.

Acknowledgements

We thank the Natural Science and Engineering Research Council and the Canada Foundation for Innovation for funding and the Laboratory for Computational Discovery (Regina; John Jorgensen, sysadmin) for supercomputer maintenance.

Appendix A. Supplementary data

Supplementary data associated with this article can be found, in the online version, at doi:10.1016/j.molcata.2011.09.028.

References

[1] A.J. Amass, T.A. McGourtey, C.N. Tuck, Eur. Polym. J. 12 (1976) 93–94.
[2] A. Sen, R.R. Thomas, Organometallics 1 (1982) 1251–1254.
[3] (a) T. Szymańska-Buzar, T. Głowiak, I. Czeluśniak, J. Organomet. Chem. 640 (2001) 72–78;
(b) T. Szymańska-Buzar, T. Głowiak, I. Czeluśniak, Polyhedron 21 (2002) 2505–2513.
[4] P.K. Baker, M.G.B. Drew, M.M. Meehan, J. Müller, Z. Anorg. Allg. Chem. 628 (2002) 1727–1729.
[5] L. Bencze, N. Bíró, B. Szabó-Ravasz, L. Mihichuk, Can. J. Chem. 82 (2004) 499–503.
[6] J.L. Hérisson, Y. Chauvin, Makromol. Chem. 141 (1971) 161–176.
[7] (a) M. Górski, T. Szymańska-Buzar, J. Mol. Catal. A 257 (2006) 41–47;
(b) M.R. Buchmeiser, D. Wang, Y. Zhang, S. Naumov, K. Wurst, Eur. J. Inorg. Chem. (2007) 3988–4000.
[8] (a) L. Bencze, A. Kraut-Vass, L. Prókai, J. Chem. Soc. Chem. Commun. (1985) 911–912;
(b) A.S. Veige, P.T. Wolczanski, E.B. Lobkovsky, Angew. Chem. Int. Ed. 40 (2001) 3629–3632.
[9] A.L.L. East, G.M. Berner, A. Morcom, L. Mihichuk, J. Chem. Theory Comput. 4 (2008) 1274–1282.
[10] J. Handzlik, M. Górski, T. Szymańska-Buzar, J. Mol. Struct. (THEOCHEM) 718 (2005) 191–201.
[11] J. Handzlik, M. Stosur, A. Kochel, T. Szymańska-Buzar, Inorg. Chim. Acta 361 (2008) 502–512.
[12] M.J. Frisch, G.W. Trucks, H.B. Schlegel, G.E. Scuseria, M.A. Robb, J.R. Cheeseman, G. Scalmani, V. Barone, B. Mennucci, G.A. Petersson, H. Nakatsuji, M. Caricato, X. Li, H.P. Hratchian, A.F. Izmaylov, J. Bloino, G. Zheng, J.L. Sonnenberg, M. Hada, M. Ehara, K. Toyota, R. Fukuda, J. Hasegawa, M. Ishida, T. Nakajima, Y. Honda, O. Kitao, H. Nakai, T. Vreven, J.A. Montgomery Jr., J.E. Peralta, F. Ogliaro, M. Bearpark, J.J. Heyd, E. Brothers, K.N. Kudin, V.N. Staroverov, R. Kobayashi, J. Normand, K. Raghavachari, A. Rendell, J.C. Burant, S.S. Iyengar, J. Tomasi, M. Cossi, N. Rega, J.M. Millam, M. Klene, J.E. Knox, J.B. Cross, V. Bakken, C. Adamo, J. Jaramillo, R. Gomperts, R.E. Stratmann, O. Yazyev, A.J. Austin, R. Cammi, C. Pomelli, J.W. Ochterski, R.L. Martin, K. Morokuma, V.G. Zakrzewski, G.A. Voth, P. Salvador, J.J. Dannenberg, S. Dapprich, A.D. Daniels, Ö. Farkas, J.B. Foresman, J.V. Ortiz, J. Cioslowski, D.J. Fox, GAUSSIAN09, Revision B.01, Gaussian Inc., Wallingford, CT, 2009.
[13] A.D. Becke, Phys. Rev. A 38 (1988) 3098–3100.
[14] (a) J.P. Perdew, Phys. Rev. B 33 (1986) 8822–8824;
(b) J.P. Perdew, Phys. Rev. B 34 (1986), 7406–7406.
[15] A.D. Becke, J. Chem. Phys. 98 (1993) 5648–5652.
[16] C. Lee, W. Yang, R.G. Parr, Phys. Rev. B 37 (1988) 785–789.
[17] J. Baker, J. Comput. Chem. 7 (1986) 385–395.
[18] C. Peng, P.Y. Ayala, M.J. Frisch, H.B. Schlegel, J. Comput. Chem. 17 (1996) 49–56.
[19] G. Scalmani, M.J. Frisch, J. Chem. Phys 132 (2010) 114110–114116.

[20] E.K. Tosh, M.Sc. Thesis, University of Regina, Regina, Canada, 2006.
[21] A.R. Fraser, P.H. Bird, S.A. Bezman, J.R. Shapley, R. White, J.A. Osborn, J. Am. Chem. Soc. 95 (1973) 597–598.
[22] M.J. Doyle, J. McMeeking, P. Binger, J. Chem. Soc. Chem. Commun. (1976) 376–377.
[23] A. Stockis, R. Hoffman, J. Am. Chem. Soc. 102 (1980) 2952–2962.
[24] R.J. McKinney, D.L. Thorn, R. Hoffman, A. Stockis, J. Am. Chem. Soc. 103 (1981) 2595–2603.
[25] C.N. Rowley, E.F. van der Eide, W.E. Piers, T.K. Woo, Organometallics 27 (2008) 6043–6045.
[26] M. Brookhart, M.L.H. Green, G. Parkin, Proc. Nat. Acad. Sci. 104 (2007) 6908–6914.